J Neuropathol Exp Neurol
Vol. 76, No. 12, December 2017, pp. 1000–1007
doi: 10.1093/jnen/nlx088

ORIGINAL ARTICLE

LBH589 Inhibits Glioblastoma Growth and Angiogenesis Through Suppression of HIF-1α Expression

Zhi-Gang Yao, PhD, Wen-Huan Li, PhD, Fang Hua, PhD, Hong-Xia Cheng, PhD, Miao-Qing Zhao, PhD, Xi-Chao Sun, PhD, Ye-Jun Qin, PhD, and Jia-Mei Li, PhD

Abstract

Glioblastoma (GBM) is an angiogenic malignancy with a highly unfavorable prognosis. Angiogenesis in GBM represents an adaptation to a hypoxic microenvironment and is correlated with tumor growth, invasion, clinical recurrence, and lethality. LBH589 (also called panobinostat) is a histone deacetylase (HDAC) inhibitor with potent antitumor activity. In the current study, we investigated the mechanism and effects of LBH589 on GBM growth and hypoxia-induced angiogenesis in vitro and in vivo. To determine the antitumor and angiogenesis activity and mechanism of LBH589, we used cell proliferations in vitro and GBM xenografts in vivo. To clarify mechanisms of LBH589 on angiogenesis, HDAC assay, RT-PCR, Western blot, and co-immunoprecipitation assays were performed. We found LBH589 displayed significant antitumor effects on GBM as demonstrated by inhibited cell proliferation, slower tumor growth, and decreased microvessel density of subcutaneous xenografts. These actions of LBH589 resulted from the disruption of heat shock protein 90/HDAC6 complex, increased HIF-1α instability and degradation, and decreased VEGF expression. Our results indicate the potential antiangiogenic activity of LBH589 in human GBM and provide some preclinical data to warrant further exploration of HDAC inhibitors for the treatment of advanced glioma. Moreover, our study supports the role of HDAC inhibitors as a therapeutic strategy to target tumor angiogenesis.

Key Words: Angiogenesis, Glioblastoma, Histone deacetylase (HDAC), Hypoxia-inducible factor 1 (HIF-1α), Panobinostat.

INTRODUCTION

Glioblastoma (GBM) is the most common and aggressive primary brain tumor, with a median overall survival of only 10–14 months (1). Despite decades of research into its treatment, prognosis remains poor, with only 3%–5% of patients surviving >3 years (2). Treatment of GBM consists of maximal surgical resection, radiotherapy, and adjuvant chemotherapy with temozolomide (3). Regardless of multimodality treatment, recurrence or progression of disease is inevitable and uniformly fatal. Therefore, it is necessary to develop effective, novel therapies for GBM.

Angiogenesis is one of the key features of GBM. Neoangiogenesis of GBM is a crucial factor in their growth, aggressive behavior, clinical recurrence, and prognosis of patients (4). Hypoxia-inducible factor 1 (HIF-1) is an important transcription factor that responses to hypoxia to regulate angiogenesis, cellular survival, and tumor invasion (5). As a subunit of HIF-1, HIF-1α is responsible to its oxygen sensitivity, determining the availability of HIF-1. HIF-1 activates a large battery of genes, including vascular endothelial growth factor (VEGF), a highly potent cytokine known to promote angiogenesis and increase oxygen delivery to hypoxic regions (6). Recently, HIF-1α and its signaling pathway have become targets for GBM chemotherapy aimed at inhibiting angiogenesis (7). For example, it has been demonstrated that histone deacetylase (HDAC) 6 contributed to HIF-1α stability indirectly through deacetylation of heat shock protein (Hsp) 90, which enhanced the Hsp90 chaperone function toward its client proteins, including HIF-1α (8, 9). Therefore, we speculated HDAC inhibitors might inhibit the deacetylase activity of HDAC6 and indirectly decrease HIF-1α expression through Hsp90/HDAC6-HIF-1α pathway.

LBH589 is a hydroxamic acid and shows its potent inhibitory activity against all class I (including HDAC1, 2, 3, 8), II (including HDAC4, 5, 6, 7, 9, 10), and IV (HDAC11) purified recombinant HDAC enzymes at low nanomolar concentrations (10). LBH589 was also at least 10-fold more potent as a HDAC inhibitory compared with vorinostat, which showed antitumor activity in GBM as a pan-HDAC inhibitor (10, 11). So far, cotreatments or single-drug treatments with LBH589 exhibited significantly in vitro and in vivo antitumor effects across a variety of hematologic malignancies and solid tumors, including diffuse large B-cell lymphoma, Hodgkin lymphoma, multiple myeloma, pancreatic cancer,

From the Department of Pathology (Z-GY, H-XC, M-QZ, X-CS, Y-JQ, J-ML) and Department of Chemotherapy (W-HL), Shandong Provincial Hospital Affiliated to Shandong University, Jinan, China; and Department of Rheumatology and Clinical Immunology, Peking Union Medical College Hospital, Chinese Academy of Medical Sciences and Peking Union Medical College, Beijing, China (FH).

Send correspondence to: Jia-Mei Li, PhD, Department of Pathology, Shandong Provincial Hospital Affiliated to Shandong University, No. 324 Jingwu Road, Jinan 250021, China; E-mail: lijiamei366@126.com

This study was supported by the National Natural Science Foundation of China (NSFC) (81402479) and Shandong Provincial Natural Science Foundation (ZR2014HM002).

The authors have no duality or conflicts of interest to declare.

and nonsmall cell lung cancer (12–14). However, the effect of LBH589 on GBM has not been reported in preclinical studies.

In this study, we detected the antitumor activity of LBH589 in vitro and in vivo against human GBM U87MG and U251MG cells using either cell proliferation assay or nude mouse xenograft model. The correlation between deacetylation activity of LBH589 and its effects on tumor growth and angiogenesis was also evaluated in vitro and in vivo.

MATERIALS AND METHODS

Cell Culture and Reagents

The U87MG and U251MG human GBM cell lines were purchased from R&S Biotechnology Co., Ltd. (Shanghai, China) and cultured in DMEM medium (Gibco BRL, Gaithersburg, MD) with 10% fetal bovine serum. For normoxic conditions, cells were incubated in an atmosphere of 5% CO_2 and 20% O_2. For hypoxic treatment, the cells were incubated in an atmosphere of 1% O_2, 5% CO_2, and 94% N_2 under intermittent flushing with nitrogen. LBH589 was obtained from Selleck Chemicals (Shanghai, China) and dissolved in dimethyl sulfoxide (DMSO) for the preparation of stock solutions (50 mM).

Cell Proliferation Assays

Cell proliferation after treatment with LBH589 at different concentrations (10, 20, and 40 nM) was measured by CCK-8 assay (Dojindo, Shanghai, China). The U87MG and U251MG cells were seeded at a density of 5×10^4 cells/100 μL DMEM/well in 96-well plates and were allowed an overnight period for attachment. Cells were incubated in a humidified incubator under hypoxic conditions at 37 °C for 24, 48, and 72 hours. After the designated time, CCK-8 solution was added to each well containing 100 μL of the culture medium and was incubated for another 4–5 hours at 37 °C. The amount of formazan dye was measured at 450 nm absorbance using Multiskan MK3 microplate reader (Thermo Scientific, Rockford, IL). All experiments were performed in triplicate and repeated 3 times.

Animal Experiments

Ten 6-week-old male athymic nude C57/BL6J mice (Wanleibio, Shenyang, China) were housed under pathogen-free conditions. All animal studies were done according to the protocol approved by the Animal Care and Use Committee at the Shandong University. U87MG tumor cells (1×10^7 cells in 200 μL medium) were injected subcutaneous into the right flank. The tumor volume was measured using a vernier caliper every 3 days and tumor volumes were calculated using the ellipsoid formula: length × width × height × 0.52 (15). At 13 days after implantation of tumor cells (tumor volume 100–300 mm^3), 5 mice were injected intraperitoneally with LBH589 (20 mg/kg/day). Likewise, the other 5 mice were injected intraperitoneally with DMSO. After injection for 4 weeks, animals were killed and tumor volume and weight were recorded. The tumor tissues were fixed with 10% buffered formalin and embedded in paraffin, then cut into 5-μm-thick sections on glass slides. Paraffin sections were dewaxed and conventional hematoxylin and eosin (H&E) staining was carried out using standard histologic procedures. For immunohistochemistry, dewaxed sections were incubated with primary antibodies against CD34 (1:200, ZSGB-Bio, Beijing, China) overnight at 4 °C. Detection of bound antibodies was done using the EnVision System (Dako, Denmark) following the manufacturers' instructions. The microvessel density (MVD) was determined by counting the number of blood vessels stained with the antiCD34 antibody. The MVD for each tumor was expressed as the average count of the 10 most densely stained fields identified in the ×200 field (16). Each positive endothelial cell cluster of immunoreactivity in contact with the selected field was counted as an individual vessel in addition to the morphologically identifiable vessels with a lumen.

HDAC Activity Assay

HDAC activity assays were performed using the colorimetric HDAC activity assay from BioVision (BioVision, San Francisco, CA) according to manufacturer's instructions and previous described (17). Briefly, 50 μg of cellular extracts from LBH589 treated hypoxic U87MG and U251MG cells were diluted in 85 μL ddH_2O; then, 10 μL of 10× HDAC assay buffer were added followed by additional of 5 μL of the colorimetric substrate; samples were incubated at 37 °C for 1 hour. Subsequently, the reaction was stopped by adding 10 μL of lysine developer and left for additional 30 minutes at 37 °C. Samples were then quantitated using Multiskan MK3 microplate reader (Thermo Fisher Scientific) at 400 nm. HDAC activity was expressed as relative OD values per μg of protein sample. The kit contains negative and positive controls that consist of nuclear extract of HeLa treated or not with Trichotatin A, respectively.

Quantitative Real-Time Reverse Transcription PCR

Total RNA was extracted from LBH589 treated hypoxic U87MG cells and quantified using RNA Isolation Reagent kit (BioTeke, Beijing, China). cDNA was obtained from 1 μg of total RNA from each sample (Super M-MLV reverse transcriptase, BioTeke) and 1 μL of cDNA sample was used as template for PCR with SYBR Green One Step RT-qPCR Kit (Solarbio, Beijing, China) following the manufacturer's instructions. PCR were carried out in an Exicycler 96 (Bioneer, Dajeon, Korea). For each sample and experiment, triplicates were made and normalized by β-actin mRNA levels. PCR amplification was performed with the following primers: HIF-α forward, 5′-GCCACATCATCACCATATAGAG-3′, reverse, 5′-TCAAAGCGACAGATAACACG-3′; VEGF forward, 5′-ACACACCCACCCACATACATA-3′, reverse, 5′-ACTCAAGTCCACAGCAGTCAA-3′; HDAC6 forward, 5′-TGGCTATTGCATGTTCAACCA-3′, reverse, 5′-GTCG AAGGTGAACTGTGTTCCT-3′; β-actin forward, 5′-CTTAG TTGCGTTACACCCTTTCTTG-3′, reverse, 5′-CTGTCACC TTCACCGTTCCAGTTT-3′.

Western Blot Analysis and Co-Immunoprecipitation

Total proteins were extracted from LBH589 treated hypoxic U87MG cells using lysis buffer (Beyotime, Wuhan, China). Western blot analyses were carried out according to methods as previously described (18). The monoclonal or polyclonal antibodies were purchased from Abcam (Cambridge, UK; antibodies against HIF-1α, acetylated lysine, HDAC6, and acetylated H3/H3), Santa Cruz Biotechnology (Santa Cruz, Santa Cruz, CA; antibody against Hsp90). Co-immunoprecipitation was performed as previously described (18). In brief, cell lysates (500 μg) were incubated with HIF-1α, Hsp90, or normal rabbit IgG, or normal mouse IgG monoclonal antibodies (Santa Cruz Biotechnology) for 1 hour, then immunoprecipitated out with Protein A-agarose beads (Santa Cruz Biotechnology) at 4 °C overnight. The immunoprecipitates were washed 3 times in the lysis buffer, and proteins were eluted with the SDS sample loading buffer prior to Western blot analyses with specific antibodies against acetylated lysine (Ace-lysine) and HDAC6.

Statistical Analysis

Data were analyzed using SPSS software (SPSS Inc., Chicago, IL). For 2 groups in the animal experiment, the Student's *t* test was used with equal/unequal variance version depending on variance ratio test. For 3 or more groups, Levene tests were performed to assess variance homogeneity. Standard 1-way ANOVA followed with Student–Newman–Keuls multiple comparison procedures were performed with homogeneous variances, and the Welch's ANOVA followed by Games–Howell multiple comparisons test was performed with heterogeneous variances. A final value of $p < 0.05$ was considered significant. GraphPad Prism 5 (GraphPad Software Inc., La Jolla, CA) was used to generate histograms and line chart.

RESULTS

LBH589 Inhibited Growth of U87MG and U251MG Cells In Vitro and In Vivo

After treatment with serial dilutions (10, 20, and 40 nM) at different times (24, 48, and 72 hours), the antitumor activity of LBH589 was assessed in human GBM U87MG and U251MG cell lines. Under phase-contrast microscope, the number of LBH589 treated U87MG cells was significantly decreased at 48 and 72 hours (Fig. 1A). The CCK-8 assay showed the relative concentration of DMSO (≤0.1%) has little influence on cell proliferation compared with the control group ($p > 0.05$). However, treatment with LBH589 resulted in significant inhibition of U87MG cell proliferation at concentrations of 20 and 40 nM at both 48 and 72 hours compared with DMSO treatment (Fig. 1B). In detail, after LBH589 treatment for 40 nM, the OD values were decreased by 57.6% ($p = 0.000$) and 52.2% ($p = 0.000$) at 48 and 72 hours, respectively. On the basis of the growth inhibition assay, the IC50 of LBH589 treatment at 48 and 72 hours was calculated to be 35 nM and 50 nM in U87MG cells. However, no significant inhibition of U87MG cells proliferation was observed after 24 hours treatment of LBH589 ($p > 0.05$). These results showed LBH589 inhibited U87MG cells proliferation.

We also detected the effect of LBH589 on the proliferation of U251MG cells. The densities of cells were also significantly decreased at 48 and 72 hours (Fig. 1A). After 24 hours, the OD value were significantly decreased by 30.0% for 40 nM group compared with DMSO treatment ($p = 0.000$, Fig. 1C). After treatment with LBH589 for 48 and 72 hours at 3 concentrations (10, 20, and 40 nM), U251MG cell proliferations were significantly inhibited compared with DMSO treatment ($p < 0.01$, Fig. 1C). For example, the OD values at 40 nM groups were decreased by 29.5% at 48 ($p = 0.000$) and 72 hours ($p = 0.000$). Our results also displayed LBH589 inhibited U251MG cells proliferation.

Nude mice bearing U87MG xenografts were treated intraperitoneally with LBH589 (20 mg/kg/day) beginning on day 13 after tumor implantation. The tumor volume was significantly smaller from the day 25 than controls that had received DMSO ($p < 0.01$, Fig. 2A, B). On day 42, LBH589 suppressed tumor growth by 53.1% ($p = 0.001$) in volume. These data indicate that LBH589 inhibited tumor growth in vivo.

LBH589 Inhibited Angiogenesis in U87MG Xenografts

We detected the MVD in the tumor tissues from the U87MG xenograft mice. Immunohistochemical staining using antibody against CD34 showed the MVD in the solid areas of the tumor was significantly reduced by 63.0% in LBH589 treatment group ($p = 0.001$, Fig. 3A, C). H&E staining showed significant tumor necrosis in both groups. Moreover, H&E staining presented numerous dilating blood vessels surrounding necrosis foci in DMSO treated tumors, while only a few vessel fissures were found in LBH589 treated tumors (Fig. 3B). Immunostaining using antiCD34 antibody showed the MVD surrounding necrosis foci was significantly reduced by 86.1% compared with the DMSO treatment controls ($p = 0.000$, Fig. 3C). These results indicated that LBH589 inhibited angiogenesis in U87MG xenografts.

LBH589 Inhibited HDACs Activity in U87MG and U251MG Cells

To investigate whether a decrease in deacetylase activity could be achieved by LBH589 treatment in U87MG and U251MG cells, total HDACs activity was evaluated in cell extracts by colorimetric commercial HDACs activity assay. As shown in Figure 4A, after LBH589 treatment for 48 hours in U87MG cells, HDACs activity was significantly decreased by 83.2% ($p = 0.022$), 90.2% ($p = 0.019$), and 98.1% ($p = 0.016$) in the corresponding treatment groups (10, 20, and 40 nM) compared with DMSO treatment group. Additionally, HDACs activity was also significantly decreased by 76.5% ($p = 0.023$), 92.6% ($p = 0.024$), and 93.0% ($p = 0.033$) in 10, 20, and 40 nM groups after treatment for 48 hours in U251MG cells. Our results indicated LBH589 inhibited HDAC activity in U87MG and U251MG cells.

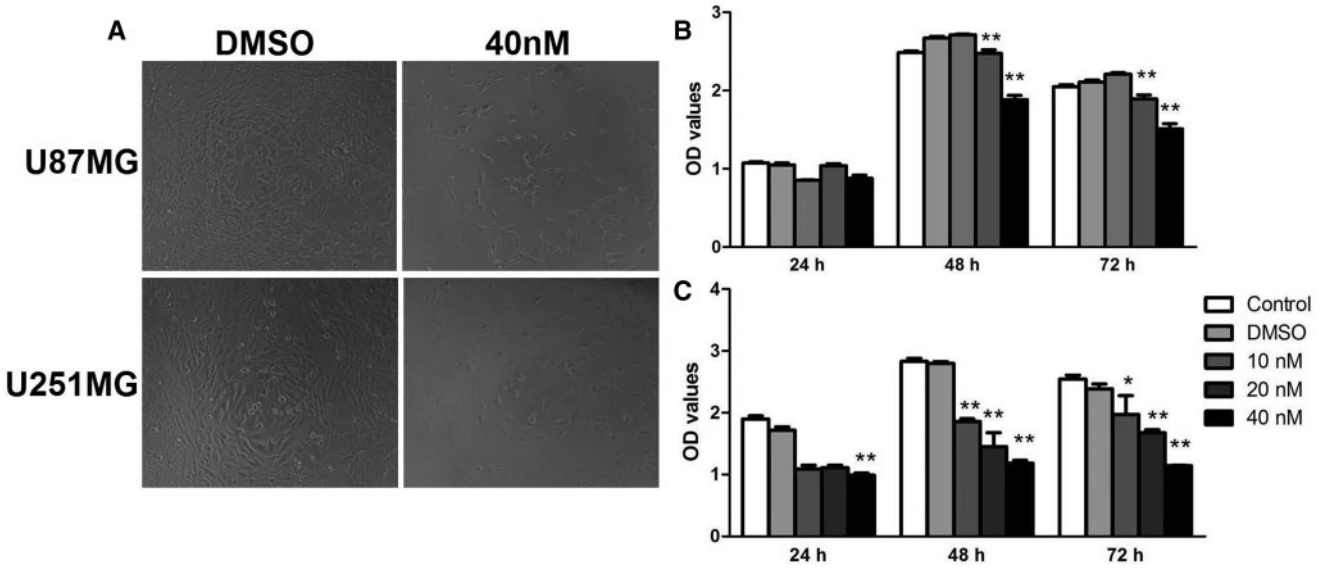

FIGURE 1. LBH589 inhibited the growth of U87MG and U251MG cells in vitro. **(A)** Representative photomicrography of U87MG and U251MG cells treated by DMSO and LHB589 (40 nM) for 48 hours. **(B)** U87MG cells were treated with 10, 20, and 40 nM of LBH589 for 24, 48, and 72 hours, and cell viability was determined using the CCK-8 assay. **(C)** U251MG cells were treated with 10, 20, and 40 nM of LBH589 for 24, 48, and 72 hours. OD: optical density. *$p < 0.05$; **$p < 0.01$; $n = 3$.

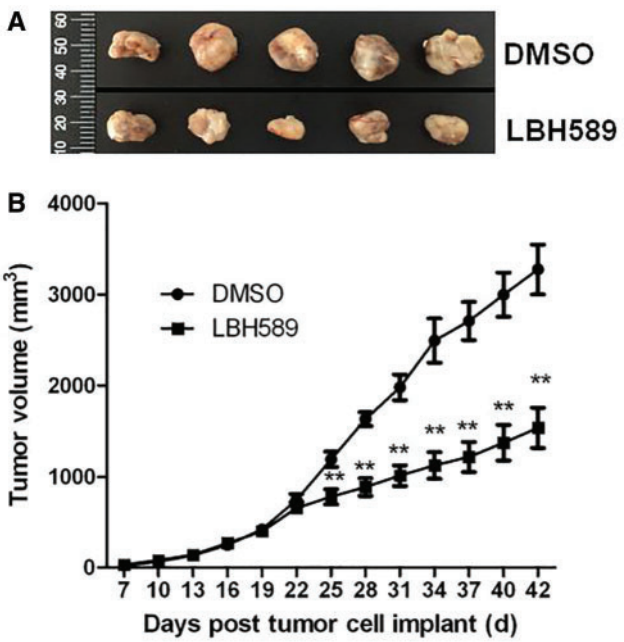

FIGURE 2. LBH589 inhibited the growth of U87MG tumor xenografts in nude mice. **(A)** Representative volume of xenograft nodules in the DMSO and LBH589 treatment animals on day 42. **(B)** Growth curves of xenografts showing the mean volume (with SEM) of both treatment groups. Mice were injected intraperitoneally with LBH589 (20 mg/kg/day) from the day 13. **$p < 0.01$; $n = 5$.

We next detected the protein deacetylation level in U87MG cells. As shown in Figure 4B, the acetylation level of histone H3 was increased after LBH589 treatment for 48 hours. The relative levels of acetylated histone H3 were significantly increased by 45.9% ($p = 0.004$), 68.3% ($p = 0.003$), and 122.3% ($p = 0.000$) in the 10, 20, and 40 nM of LBH589 treatment groups compared with the DMSO group, respectively. LBH589 also increased the acetylation level of tubulin by 87% ($p = 0.03$) and 142% ($p = 0.004$) in the 20 nM and 40 nM treatment cells, respectively. These results suggested LBH589 inhibited deacetylation of nuclear and cytoplasmic proteins in U87MG cells.

Mechanisms of LBH589 Inhibited Angiogenesis in U87MG Cells

Considering the important role of HIF-1α and VEGF in angiogenesis of GBM (7), we first detected HIF-1α and VEGF expressions at mRNA and protein levels after LBH589 treatment for 48 hours under hypoxic conditions. Compared with DMSO treatment group, VEGF mRNA expression was reduced by 50.7% in LBH589 treatment group ($p = 0.026$, Fig. 5A). However, no significant difference of HIF-1α mRNA level was observed between DMSO and LBH589 treatment groups ($p = 0.035$). At protein levels, LBH589 treatment significantly reduced HIF-1α and VEGF expressions by 93.8% ($p = 0.000$) and 75.7% ($p = 0.001$), respectively (Fig. 5B). These results suggested HIF-1α may be regulated by LBH589 at the posttranslational level.

Previous studies have demonstrated that HIF-1α degradative pathway was regulated by Hsp90 (19). Accordingly, co-immunoprecipitation with immunoblotting analysis showed HIF-1α coprecipitated the decreased level of Hsp90 in U87MG cells after LBH589 treatment for 48 hours under hypoxia compared with the DMSO group (Fig. 5C). However, there was no significant difference of HDAC6 expression between the 2 groups. Second, HDAC6 has been demonstrated to interact with Hsp90 and regulate its acetylation (8).

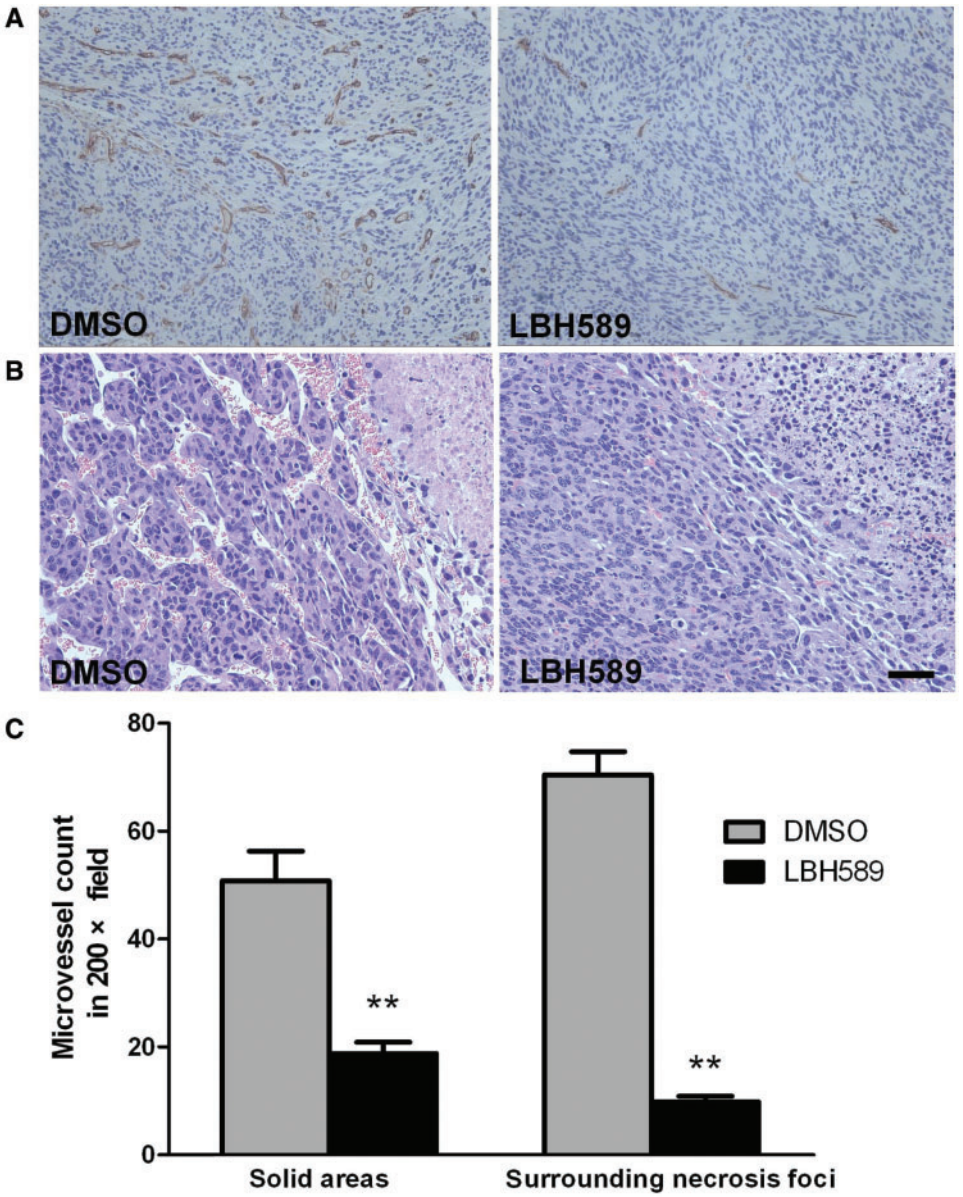

FIGURE 3. LBH589 inhibited angiogenesis in U87MG xenografts. **(A)** Immunohistochemistry with antibodies against the endothelial cell marker (CD34) in the solid areas of the tumor. **(B)** The dilating blood vessels and vessel fissures surrounding necrosis foci (upper right corner) in DMSO and LBH589 treated tumors visualized clearly by H&E staining. Bar = 200 μm. **(C)** Decreased MVD in LBH589 treated xenografts. **$p < 0.01$; $n = 5$.

Therefore, we next determined whether HDAC activity inhibition caused an increase in Hsp90 acetylation. Co-immunoprecipitation with immunoblotting analysis showed Hsp90 coprecipitated with the increased level of acetylated lysine residues (Ace-lysine) and the decreased level of HDAC6 compared with the DMSO group (Fig. 5D), indicating that Hsp90/HDAC6 complex formation was disrupted by LBH589. However, there was no difference of HDAC6 mRNA or protein expression level between both groups (data not shown). These results showed that LBH589 inhibited HDAC6-mediated deacetylation of Hsp90, resulting in HIF-1α instability and degradation.

DISCUSSION

In this study, we found LBH589 significantly inhibited the proliferations of U87MG and U251MG cells in vivo. In addition, LBH589 also significantly suppressed growth of U87MG xenografts in vitro. These results suggest antitumor potency of LBH589 on GBM. GBM is also one of the most highly vascularized human tumors, and its growth and survival is dependent on angiogenesis (4). HIF-1α is one of the best described regulatory gene and transcription factor activated under hypoxia, leading to VEGF transcription and angiogenesis in GBM (20). VEGF increases vascular endothelial cell proliferation in GBM. Multiple strategies have been developed to

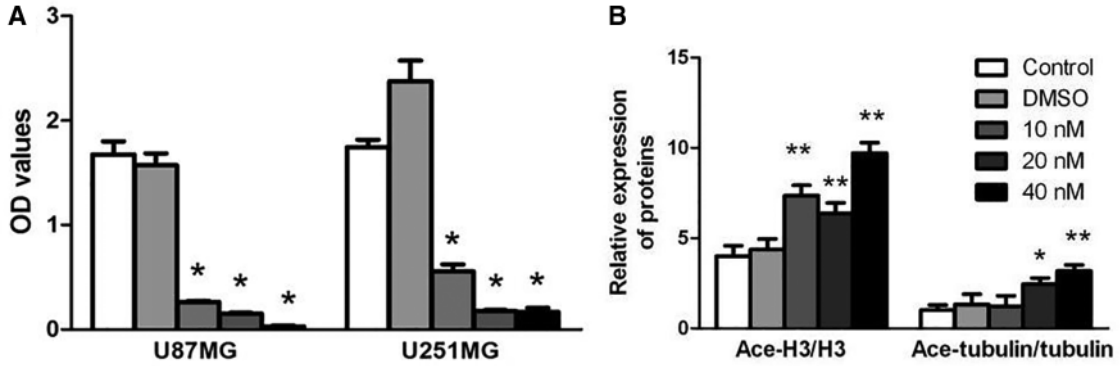

FIGURE 4. Forty nanomolar of LBH589 inhibited HDACs activity and protein deacetylation in GBM cell lines. **(A)** HDAC activity detected in U87MG and U251MG cells and expressed as optical densities (ODs). **(B)** Relative expressions of acetylated (Ace-) H3 histones and tubulin detected by Western blot. *$p < 0.05$; **$p < 0.01$; $n = 4$.

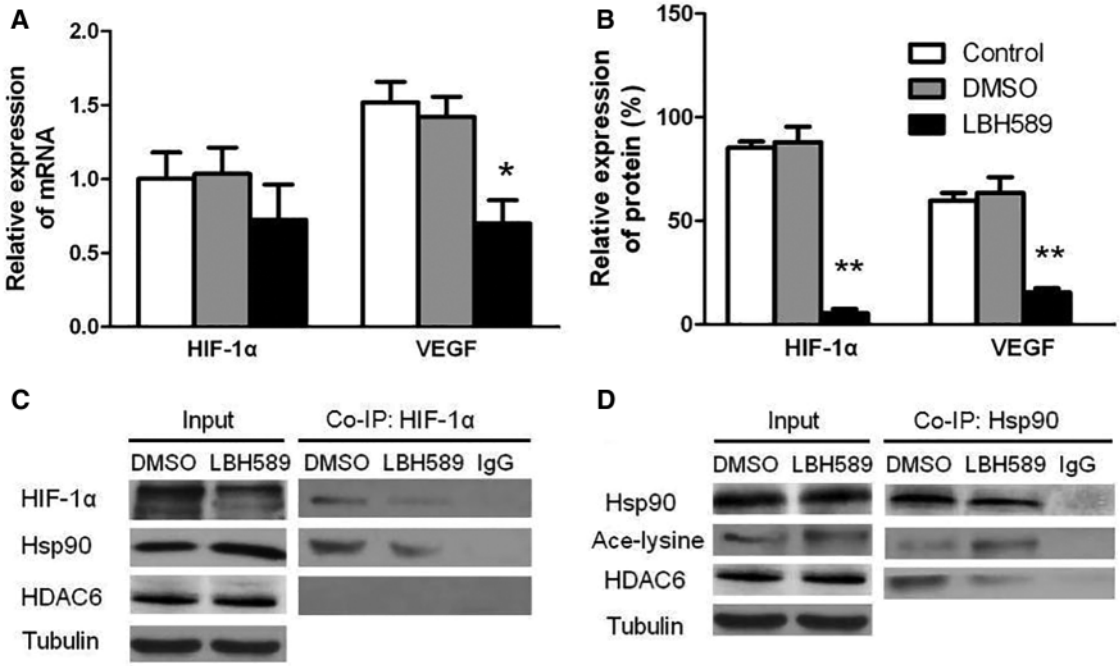

FIGURE 5. Forty nanomolar of LBH589 inhibited HIF-1α and VEGF expressions through disrupting Hsp90/HDAC6 complex after treatment for 48 hours. **(A)** Expressions of HIF-1α and VEGF mRNA in U87MG cells under hypoxic conditions. **(B)** Expressions of HIF-1α and VEGF protein in U87MG cells. **(C)** Effects of LBH589 on complex formation between HIF-1α and Hsp90. Co-immunoprecipitation (Co-IP) with antibody to HIF-1α and Western blot with antibodies to HIF-1α, Hsp90, and HDAC6. **(D)** Effects of LBH589 on complex formation between acetylated Hsp90 and HDAC. Hsp90 was the co-immunoprecipitation antibody, and Western blot antibodies included Hsp90, Ace-lysine, and HDAC6.

target VEGF-mediated angiogenesis (21). In our study, we found LBH589 inhibited HIF-1α at the protein level rather than the mRNA level under hypoxic conditions. LBH589 inhibited VEGF at both protein and mRNA levels. Therefore, the anti-angiogenesis effect of LBH589 was confirmed by the inhibition of HIF-1α activity and decreased VEGF secretion in our study. Furthermore, Zhong et al found the HIF-1α immunostaining was especially intense in pseudopalisading tumor cells surrounding areas of necrosis in human GBM specimens (22), suggesting the increased proangiogenic factors surrounding the necrosis foci. Actually, microvascular hyperplasia in the GBM is a form of angiogenesis that is induced by hypoxic pseudopalisading cells and is usually present in regions adjacent to necrosis (23). Hence, the significantly decreased MVD detected in implanted U87MG xenografts, especially surrounding necrosis foci, provided further evidence that LBH589 inhibits hypoxia-induced angiogenesis in GBM.

It has been demonstrated HDAC6 contributed to HIF-1α stability indirectly through deacetylation of Hsp90, which enhanced the Hsp90 chaperone function toward its client proteins, including HIF-1α (8, 9). On the other hand, in our study, although there was no effect on HDAC6 expression, LBH589

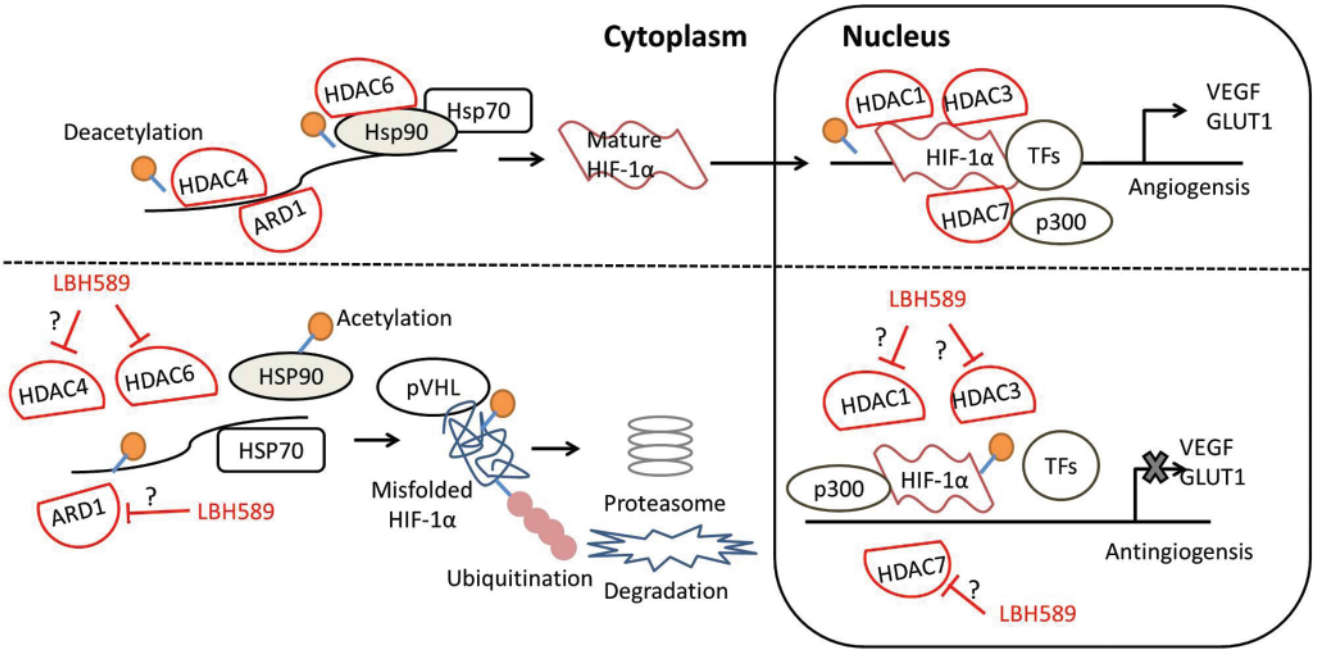

FIGURE 6. The potential HDAC targets for LBH589 to inhibit the activity of HIF-1α in glioblastic cells under hypoxia conditions. The schematic diagram above the dotted line shows HDAC4 (26) and/or ARD1 (28) enhances HIF-1α stability through HIF-1α protein lysine acetylation in the cytoplasm. In the cell nucleus, HDAC1 and 3 (24) and/or HDAC7/p300 (27) directly bind with HIF-1α to enhance HIF-1α stability and transcriptional activity, resulting in expression of proangiogenic factors, such as VEGF. The schematic diagram below the dotted line shows LBH589 may target these HDACs abovementioned to inhibit the activity of HIF-1α. Our study has demonstrated LBH589 inhibits HDAC6 activity and increases Hsp90 acetylation, resulting in misfolding and subsequent degradation of HIF-1α protein. The question marks represent other potential HDAC targets for LBH589 to inhibit the activity of HIF-1α. These targets remain to be confirmed in the future studies.

significantly inhibited HDAC activity in U87MG and U251MG cells and increased protein acetylation in U87MG cells, suggesting LBH589 may exert its inhibitory effects on GBM through decreased HDAC6 activity. Accordingly, the loss of deacetylation activity of HDAC6 induced by LBH589 increased the level of acetylated Hsp90 detected using co-immunoprecipitation. The hyperacetylation of Hsp90 repressed its chaperone function, leading to the accumulation of immature HIF-1α and degradation mediated by the von Hippel–Lindau (VHL) protein, a tumor suppressor that acted as an ubiquitin ligase (E3) to enhance HIF-1 ubiquitination and proteasomal degradation (24). Thus, we speculated LBH589 may inhibit angiogenesis through targeting HDAC6 activity in the Hsp90/HDAC6 complex and facilitating HIF-1 degradation (Fig. 6). In addition, it has been reported HDAC1, 3, and 4 could directly bound to HIF-1α and induced deacetylation of lysine residues and thus enhanced HIF-1α stability (25, 26). HDAC7 also cotranslocated to the nucleus with HIF-1α under hypoxic conditions and increased transcriptional activity of HIF-1α through the formation of a complex with HIF-1α and p300 (27). Jeong et al reported that HIF-1α protein was acetylated at the K532 residue by ARD1 (Arrest-Defective-1), promoting its interaction with VHL and thus enhancing its ubiquitination and degradation (27). These findings suggest multiple Class I and Class II HDACs regulate HIF-1α stability as demonstrated in Figure 6. Thus, it cannot be excluded that LBH589, as a pan-HDAC inhibitor, may also decrease HIF-1α levels through simultaneously targeting other HDACs. On the other hand, it has been demonstrated LBH589 inhibited VEGF-induced endothelial cell motility and tube formation detected using human umbilical vein endothelial cells (29). These results provide evidence that LBH589 might inhibit angiogenesis in GBM through targeting both the tumor and stromal endothelial cell compartments. Thus, further research is needed to understand other pathways which act simultaneously to enhance antiangiogenic effects of LBH589 in GBM.

In conclusion, we found LBH589 inhibited proliferation and angiogenesis of GBM both in vivo and in vitro through increased HIF-1α instability and degradation mediated by Hsp90/HDAC6 complex under hypoxic conditions. Although a recent phase II study reported the addition of LBH589 to bevacizumab did not significantly improve the 6-month progression-fee survival rate of patients with recurrent GBM compared with historical controls of bevacizumab monotherapy (30), we think our study will provide some preclinical data exploring the activity of the LBH589 to potentially improve the therapeutic response for GBM in the future.

REFERENCES

1. Johnson DR, O'Neill BP. Glioblastoma survival in the United States before and during the temozolomide era. J Neurooncol 2012;107:359–64
2. Krex D, Klink B, Hartmann C, et al. Long-term survival with glioblastoma multiforme. Brain 2007;130:2596–606

3. Yoo RE, Choi SH, Kim TM, et al. independent poor prognostic factors for true progression after radiation therapy and concomitant temozolomide in patients with glioblastoma: subependymal enhancement and low ADC value. AJNR Am J Neuroradiol 2015;36:1846–52
4. Miller JJ, Wen PY. Emerging targeted therapies for glioma. Expert Opin Emerg Drugs 2016;21:441–52
5. Semenza GL. Regulation of mammalian O2 homeostasis by hypoxia-inducible factor 1. Annu Rev Cell Dev Biol 1999;15:551–78
6. Ho QT, Kuo CJ. Vascular endothelial growth factor: biology and therapeutic applications. Int J Biochem Cell Biol 2007;39:1349–57
7. Yang L, Lin C, Wang L, et al. Hypoxia and hypoxia-inducible factors in glioblastoma multiforme progression and therapeutic implications. Exp Cell Res 2012;318:2417–26
8. Kovacs JJ, Murphy PJ, Gaillard S, et al. HDAC6 regulates Hsp90 acetylation and chaperone-dependent activation of glucocorticoid receptor. Mol Cell 2005;18:601–7
9. Zhang D, Li J, Costa M, et al. JNK1 mediates degradation HIF-1alpha by a VHL-independent mechanism that involves the chaperones Hsp90/Hsp70. Cancer Res 2010;70:813–23
10. Bezecny P. Histone deacetylase inhibitors in glioblastoma: pre-clinical and clinical experience. Med Oncol 2014;31:985
11. Shao W, Growney JD, Feng Y, et al. Potent anticancer activity of the pan-deacetylase inhibitor panobinostat (LBH589) as a single agent in in vitro and in vivo tumor models. In: 99th American Association of Cancer Research Annual Meeting, April 12–16, 2008, San Diego, CA, Abstract 6244
12. Assouline SE, Nielsen TH, Yu S, et al. Phase 2 study of panobinostat with or without rituximab in relapsed diffuse large B-cell lymphoma. Blood 2016;128:185–94
13. Wahaib K, Beggs AE, Campbell H, et al. Panobinostat: a histone deacetylase inhibitor for the treatment of relapsed or refractory multiple myeloma. Am J Health Syst Pharm 2016;73:441–50
14. Jin N, Lubner SJ, Mulkerin DL, et al. A phase II trial of a histone deacetylase inhibitor panobinostat in patients with low-grade neuroendocrine tumors. Oncologist 2016;21:785–6
15. Corbeaux T, Hess I, Swann JB, et al. Thymopoiesis in mice depends on a Foxn1-positive thymic epithelial cell lineage. Proc Natl Acad Sci U S A 2010;107:16613–8
16. Ng SS, MacPherson GR, Gütschow M, et al. Antitumor effects of thalidomide analogs in human prostate cancer xenografts implanted in immunodeficient mice. Clin Cancer Res 2004;10:4192–7
17. Chavez-Blanco A, Segura-Pacheco B, Perez-Cardenas E, et al. Histone acetylation and histone deacetylase activity of magnesium valproate in tumor and peripheral blood of patients with cervical cancer. A phase I study. Mol Cancer 2005;4:22
18. Yao ZG, Liang L, Liu Y, et al. Valproate improves memory deficits in an Alzheimer's disease mouse model: investigation of possible mechanisms of action. Cell Mol Neurobiol 2014;34:805–12
19. Isaacs JS, Yun-Jin J, Mimnaugh EG, et al. Hsp90 regulates a VHL-independent HIF-1α degradative pathway. J Biol Chem 2002;33:29936–44
20. Clara CA, Marie SK, de Almeida JR, et al. Angiogenesis and expression of PDGF-C, VEGF, CD105 and HIF-1α in human glioblastoma. Neuropathology 2014;34:343–52
21. Weathers SP, de Groot J. VEGF manipulation in glioblastoma. Oncology (Williston Park) 2015;29:720–7
22. Zhong H, De Marzo AM, Laughner E, et al. Overexpression of hypoxia-inducible factor 1alpha in common human cancers and their metastases. Cancer Res 1999;59:5830–5
23. Brat DJ, Van Meir EG. Vaso-occlusive and prothrombotic mechanisms associated with tumor hypoxia, necrosis, and accelerated growth in glioblastoma. Lab Invest 2004;84:397–405
24. Qian DZ, Kachhap SK, Collis SJ, et al. Class II histone deacetylases are associated with VHL-independent regulation of hypoxia-inducible factor 1 alpha. Cancer Res 2006;66:8814–21
25. Kim SH, Jeong JW, Park JA, et al. Regulation of the HIF-1alpha stability by histone deacetylases. Oncol Rep 2007;17:647–51
26. Geng H, Harvey CT, Pittsenbarger J, et al. HDAC4 protein regulates HIF1α protein lysine acetylation and cancer cell response to hypoxia. J Biol Chem 2011;286:38095–102
27. Kato H, TamamizuKato S, Shibasaki F. Histone deacetylase 7 associates with hypoxia-inducible factor 1and increases transcriptional activity. J Biol Chem 2004; 279:41966–74
28. Jeong JW, Bae MK, Ahn MY, et al. Regulation and destabilization of HIF-1alpha by ARD1-mediated acetylation. Cell 2002;111:709–20
29. Qian DZ, Kato Y, Shabbeer S, et al. Targeting tumor angiogenesis with histone deacetylase inhibitors: the hydroxamic acid derivative LBH589. Clin Cancer Res 2006;12:634–42
30. Lee EQ, Reardon DA, Schiff D, et al. Phase II study of panobinostat in combination with bevacizumab for recurrent glioblastoma and anaplastic glioma. Neuro Oncol 2015;17:862–7